Journal of Molecular Graphics and Modelling 35 (2012) 49–56

Contents lists available at SciVerse ScienceDirect

Journal of Molecular Graphics and Modelling

journal homepage: www.elsevier.com/locate/JMGM

TDDFT studies on the structures and ECD spectra of chiral bisarylimidos bearing different lengths of o-alkoxy chain-substituted polyoxomolybdates

Jian-Ping Wang[a], Li-Kai Yan[a,*], Guo-Chun Yang[a], Wei Guan[a], Zhong-Min Su[a,b,*]

[a] Institute of Functional Material Chemistry, Faculty of Chemistry, Northeast Normal University, Changchun 130024, PR China
[b] Key Laboratory of Polyoxometalate Science of Ministry of Education, Faculty of Chemistry, Northeast Normal University, Changchun 130024, PR China

ARTICLE INFO

Article history:
Received 29 October 2011
Received in revised form
26 December 2011
Accepted 28 December 2011
Available online 4 February 2012

Keywords:
Polyoxometalates
Chirality
Charge-transfer
TDDFT
Circular dichroism spectrum

ABSTRACT

The chiroptical properties of bisarylimidos bearing o-alkoxy chain-substituted polyoxomolybdates $[Mo_6O_{17}(2,2'\text{-}NC_6H_4OC_nH_{2n}OC_6H_4N)]^{2-}$ [n = 4(**2**), 6(**3**±), 8(**4**)] were investigated using the time-dependent density functional method. The results showed that the studied chiral polyoxometalates (POMs) manifested similar absorption sites but displayed different shapes and magnitudes in their electronic circular dichroism (ECD) spectra. The ECD spectra of the studied chiral POMs originated from charge-transfer (CT) transitions from arylimido fragments to the POM cages and from oxygen atoms to the molybdenum atoms in the POM cages. The o-alkoxy chain served as a scaffold for generating chirality rather than contributing to the ECD spectrum of the studied POMs. The induced chiralities of the POM cages were defined by the CT transitions, which were completely localized on the POM cages. Furthermore, the long-range corrected CAM-B3LYP hybrid functional and a basis set that is larger than Lanl2DZ should be used for ECD calculations of chiral POMs. Our work establishes the use of computational studies to investigate the chiroptical properties of chiral POMs and provides theoretical interpretations.

1. Introduction

Polyoxometalates (POMs) are inorganic clusters that are composed of early transition metal oxides in their high valence states (usually W^{VI}, Mo^{VI}, and V^{V}). POMs have attracted much attention due to their unique physicochemical properties, including multistep redox [1], magnetic [2], conducting [3], and nonlinear optical properties [4]. The introduction of chirality into POMs makes them more attractive [5,6] because chiral POMs perform well in asymmetric catalysis [7] and chiral recognition [8,9] and often exhibit marvelous structures [10]. Many chiral POMs [11] and POM-based chiral materials [12] have been designed and synthesized. One popular approach for generating chiral POMs is through the bonding of a chiral group [13], such as a peptide [14] or metal complex [5], to the POM. In this case, the chirality transfer from the chiral group to the POM cage is significant. Recently, the subject of chiral POMs has been reviewed due to a large number of reports concerning POM-based chiral systems [15].

Chiral molecules are typically characterized by circular dichroism (CD) spectroscopy [11], which refers to the differential absorption of left and right circularly polarized light. CD spectroscopy has been applied to the study of molecular recognition and intermolecular interactions [16,17], especially in proteins and DNA [18]. Chiral POMs are often characterized by CD spectroscopy in the ultraviolet-visible (UV-Vis) region [12,19]. Absorption in this region is related to electronic excitations; therefore, CD spectra from the UV-Vis region are termed electronic CD (ECD) spectra. The ability to theoretically predict and produce ECD spectra is valuable for specifying molecular conformations in solution [20,21] and assigning the origins of the ECD spectrum [17]. For example, Ziegler and his co-workers calculated the ECD spectra of metal complexes and assigned their origins in detail [22,23]. It is especially beneficial to determine the origins of the ECD spectra of chiral POMs due to their complex geometric and electronic structures. According to our previous studies, POM-based compounds exhibited charge-transfer (CT) transitions from oxygen atoms to transition metal atoms in pure inorganic POMs [24] and from organic fragments to POM cages in organic-inorganic hybrid POMs [25,26].

The construction and/or prediction of experimental ECD spectra is a costly undertaking in that chiral molecules are commonly low symmetry (typically C_2), and a large number of excited states must be calculated [27]. Many theoretical methods have been applied to study the ECD spectra of chiral molecules, such as semi-empirical, time-dependent Hartree-Fock (HF), multireference configuration interaction, coupled cluster wave function, and time-dependent density functional theory (TDDFT) methods

* Corresponding authors. Tel.: +86 431 85099108; fax: +86 431 85684009.
E-mail addresses: yanlk924@nenu.edu.cn (L.-K. Yan), zmsu@nenu.edu.cn (Z.-M. Su).

1093-3263/$ – see front matter © 2012 Elsevier Inc. All rights reserved.
doi:10.1016/j.jmgm.2011.12.011

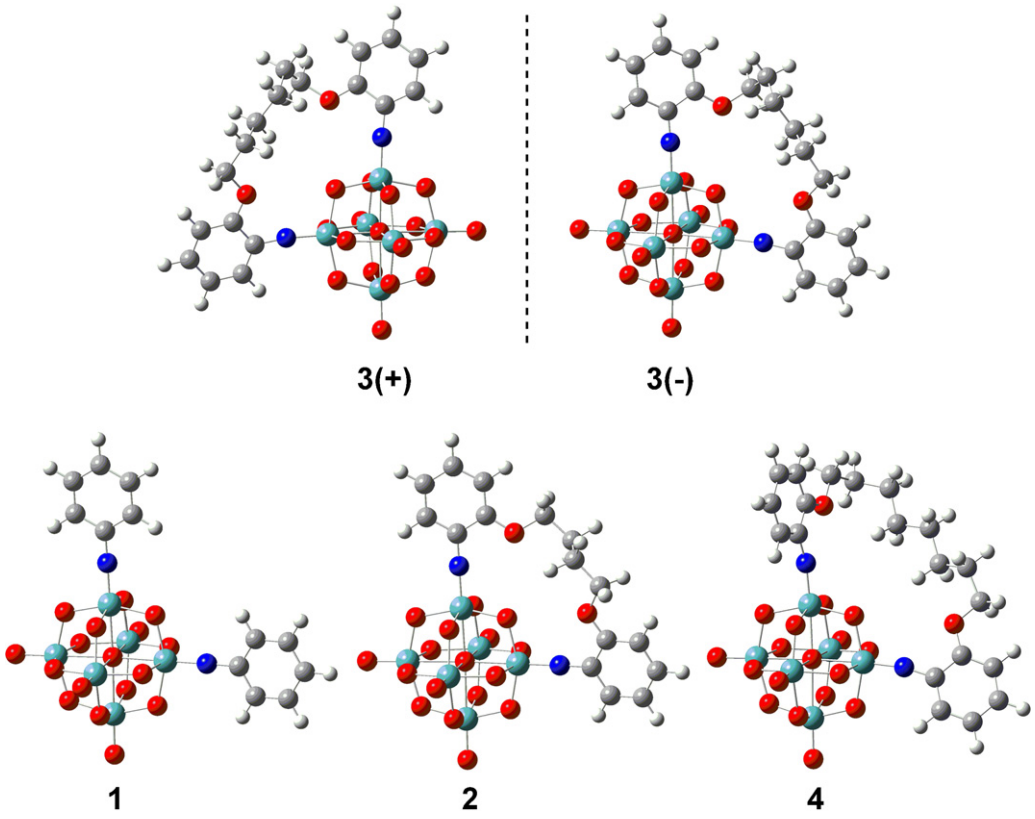

Fig. 1. The computational models of the studied chiral POMs.

[27]. Among these methods, TDDFT provides sufficient accuracy and reasonable computational cost for calculating the ECD spectra of large molecules [28] and metal complexes [29]. Furthermore, the hybrid exchange-correlation functional using the Coulomb-attenuating method (CAM-B3LYP) [30] gives satisfactory results. The CAM-B3LYP hybrid functional improves the ECD calculations of conjugated systems compared to traditional hybrid functionals such as B3LYP [31]. Valence, Rydberg, and CT excitations are well described by CAM-B3LYP, which correctly deals with the long-range asymptotic behavior using a large portion of the HF exchange functional [32–34]. The past few years have also seen many studies on the applications of CAM-B3LYP for calculating the excited properties [35–37], the bonding features [38], the electric field gradients [39], and other properties [40–42] of large metal-containing systems.

In this paper, we extend the application of CAM-B3LYP to the ECD calculations of a series of bisarylimidos bearing o-alkoxy chain-substituted Lindqvist-type polyoxomolybdates $[Mo_6O_{17}(2,2'\text{-}NC_6H_4OC_nH_{2n}OC_6H_4N)]^{2-}$ [n = 4(**2**), 6(**3**±), 8(**4**)] [43]. The calculation models for these chiral POMs (systems **2**, **3**(±), and **4**) and their parent polyanion $[Mo_6O_{17}(NC_6H_5)_2]^{2-}$ (system **1**) are shown in Fig. 1. Our goal with this study was to answer the following questions: What is the efficiency of CAM-B3LYP on the ECD calculations of chiral POMs? What are the origins of the ECD spectra of the studied chiral POMs? What types of roles do o-alkoxy chains and POM cages play in the studied chiral POMs? Does chirality transfer occur in the studied chiral POMs?

2. Computational methods

To determine an efficient computational method for geometry optimization, the geometric structure of system **2** was optimized both at the BP86/TZP level in ADF2008 [44–46] and the BP86/6-31+G*/Lanl2DZ level in Gaussian09W A02 [47]. The results showed that the optimized geometric parameters of system **2** that were obtained by ADF and Gaussian slightly deviated from each other, and those obtained by ADF were closer to the experimental values than those obtained by Gaussian (Supplementary File). Furthermore, the computational efficiency for POMs in ADF was favorable in terms of accuracy and computational cost. Thus, the geometry optimizations were performed using ADF. The local density approximation (LDA) characterized by the Vosko-Willk-Nusair (VWN) parameterization [48] for correlation was used. The generalized-gradient approximation (GGA) was employed using the Becke [49] and Perdew [50] exchange correlation (XC) functionals. The zero-order regular approximation (ZORA) [51] was adopted in all calculations to account for the scalar relativistic effects. The basis functions were Slater-type sets. Triple-ζ plus polarization basis sets were used to describe the valence electrons of all atoms except for transition metal Mo atoms that had frozen cores composed of 1s to 3spd shells, which were described by means of single Slater functions. Moreover, the value of the numerical integration parameter that was used to determine the precision of the numerical integrals was 6.0. Geometry optimization was performed in the presence of a solvent model, which was accounted for by the conductor-like screening model (COSMO) [52] implemented as part of the ADF code. To define the cavities surrounding the molecules, we used a solvent-excluding surface method and fine tesserae. The ionic radii that actually defined the size of the solvent cavity where the target molecules remained were set as 1.26 Å, 1.52 Å, 1.70 Å, 1.55 Å, and 1.20 Å for Mo, O, C, N, and H, respectively. The dielectric constant (ε) was set as 37.5 to model the solvent acetonitrile.

The ECD spectra of systems **2**, **3**(±), and **4** were calculated using the TDDFT method in Gaussian 09. According to computational method evaluations (Supplementary File) and our previous work [53], the CAM-B3LYP/Lanl2DZ [30,54,55] method proved efficient

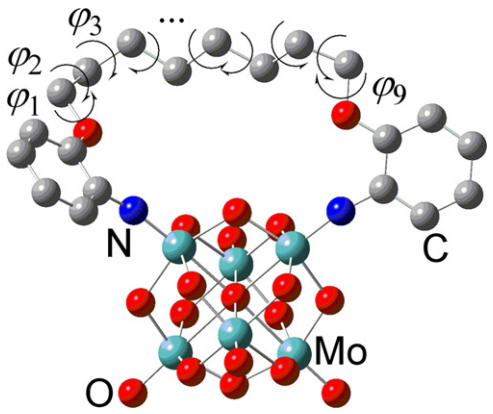

Fig. 2. The labels of the torsion angles in system **4**. The elements are indicated, but H atoms are omitted for clarity.

for the ECD calculations of chiral POMs. Solvent effects, which have been shown to significantly influence molecular ECD spectra [56,57], were considered by the polarizable continuum model (PCM) [58] using the integral equation formalism variant in acetonitrile solvent. The lowest 200 excited states were calculated to simulate the ECD spectra of systems **2**, **3**(±), and **4**.

3. Results and discussion

3.1. Geometric and electronic structures

The geometric parameters of the studied systems, which largely affect the molecular ECD spectra, were analyzed first [59,60]. The free o-alkoxy chain is achiral and quite flexible due to the facile rotations of the C-C bonds. The torsion angles of the C-C bonds in the o-alkoxy chain of system **4** are indicated in Fig. 2. There were nine torsion angles (φ_1–φ_9) in the o-alkoxy chain of system **4**, and five and seven of those torsion angles in systems **2** and **3**, respectively. These torsion angles were largely restrained in systems **2**, **3**(±), and **4,** as two terminal oxygen atoms of the o-alkoxy chain were bonded to two aromatic rings. Two arylimido rings were simultaneously stretched out of the intramolecular plane.

The calculated torsion angles are listed in Table 1, which shows that the torsion angles φ in systems **2**, **3**(±), and **4** were in reasonable agreement with the experimental values [43]. The slightly large discrepancy of φ_2 in system **2** between the calculated and the experimental values was due to the C_2 symmetry restriction during optimization. This meant that the o-alkoxy chain was relatively rigid in solution, and its geometric structure in solution was similar to that observed in a crystal. Therefore, we were convinced that the subsequent ECD calculations based on the optimized structures were acceptable for comparison with experimental values.

Table 1
The calculated torsion angles (φ_1–φ_9) (Å) in systems **2**, **3**(±), and **4**, with experimental values[a] in brackets.

	2	**3**(+)	**3**(−)	**4**
φ_1	178 (168)	−81 (−74)	80 (75)	172 (164)
φ_2	−76 (−123)	−54 (−48)	52 (48)	−74 (−84)
φ_3	175 (179)	−57 (−55)	58 (54)	85 (74)
φ_4	−76 (−46)	−171 (−150)	171 (150)	−167 (−173)
φ_5	178 (−172)	−177 (−163)	177 (178)	−174 (−171)
φ_6	–	70 (72)	−70 (−73)	−164 (−169)
φ_7	–	179 (173)	−177 (−173)	−174 (−175)
φ_8	–	–	–	−56 (−34)
φ_9	–	–	–	−175 (179)

[a] The experimental values were obtained from reference [43].

The frontier molecular orbital (FMO) energy diagrams for systems **1**, **2**, **3**(−), and **4** are shown in Fig. 3. The highest occupied molecular orbital (HOMO) of system **1** was localized on the arylimido fragments and molybdenum atoms that were bearing the nitrogen atom. The lowest unoccupied molecular orbital (LUMO) and LUMO + 1 of system **1** were nearly degenerate and were formed by the contributions of the p orbitals of the bridging oxygen atoms and the d orbitals of the molybdenum atoms in the polyanion. Compared with system **1**, the HOMO energy level of system **2** was shifted up due to the participation of the oxygen atoms in the o-alkoxy chain. The LUMO and LUMO + 1 of system **2** were similar to those of system **1**. The FMOs of systems **3(**−**)** and **4** were quite similar to those of system **2**. The energy differences between the HOMO and LUMO decreased from system **1** to systems **2**, **3**(±), and **4**. For the three chiral systems, the o-alkoxy chain did not significantly contribute to the FMOs.

3.2. Optical activities

Chiral POMs are usually large in size with low symmetry; therefore, quantum chemical studies on their excitation energies and optical rotatory strengths are limited. To the best of our knowledge, there are few theoretical studies that report the ECD calculations of chiral POMs. Herein, five methods, HF, B3LYP, CAM-B3LYP, B2PLYP, and BHandHLYP, were investigated for their efficiency in the ECD calculations of system **3(**−**)** (Supplementary File). The results showed that HF overestimated the absorption energy of the studied system, while B3LYP underestimated it. The other three hybrid functionals gave comparable results that were in accord with experimental values. The correlation functional in the DFT method and the large proportion of HF in the exchange functional improved the ECD calculations of the studied system. The long-range corrected CAM-B3LYP hybrid functional presented similar absorption sites and rotatory strengths to those that were obtained using B2PLYP and BHandHLYP. Furthermore, the basis set effect was considered by testing four differently sized basis sets (Supplementary File). The large basis set def2-TZVP [61,62] was favorable for constructing the ECD spectra of the studied systems, but the computational cost was expensive (Supplementary File). On the basis of computational method evaluations, the TDDFT/CAM-B3LYP/Lanl2DZ method was used to produce the experimental ECD spectra of systems **3**(±). The excitations that contributed to the ECD spectra over different energy ranges were specified. Then, the ECD spectra of systems **2** and **4** were predicted.

The calculated excitation energies, the oscillator strengths, and the simulated UV-Vis spectra for systems **2**, **3**(−), and **4** are shown in Fig. 4. Systems **2**, **3**(−), and **4** showed similar UV-Vis absorptions at $\Delta E \approx 3.2$ eV and $\Delta E \approx 4.8$ eV, respectively. Keeping the calculation errors caused by a small basis set in mind, we assigned the low-lying absorption of $\Delta E \approx 3.2$ eV to the experimental bands at $\Delta E \approx 3.4$ eV and 4.6 eV, while the high-lying absorption at $\Delta E \approx 4.8$ eV was assigned to the experimental bands at $\Delta E \approx 5.3$ eV and 5.6 eV [43]. For system **2,** the low-lying UV-Vis band was mainly from excited states 7, 9, and 11, and the high-lying UV-Vis band was from states 95, 98, 173, and 183. Because each of the crucial excited states was composed of several electron transitions, it was difficult to analyze the individual molecular orbitals that were involved in electronic transitions. To clarify the origins of the ECD spectra of studied systems, electron density difference maps (EDDMs) of the crucial states were calculated using the Gauss-Sum2.2.3 software package [63]. An EDDM is a representation of the changes in electron density that occur for a given electronic transition. It can be seen from the EDDMs (Supplementary File) that the excited states 7, 9, and 11 of system **2** were ascribed to CT transitions from π-bonding orbitals on the arylimido fragments to π*-antibonding orbitals between the terminal oxygen atoms and molybdenum atoms (CT^1). In contrast,

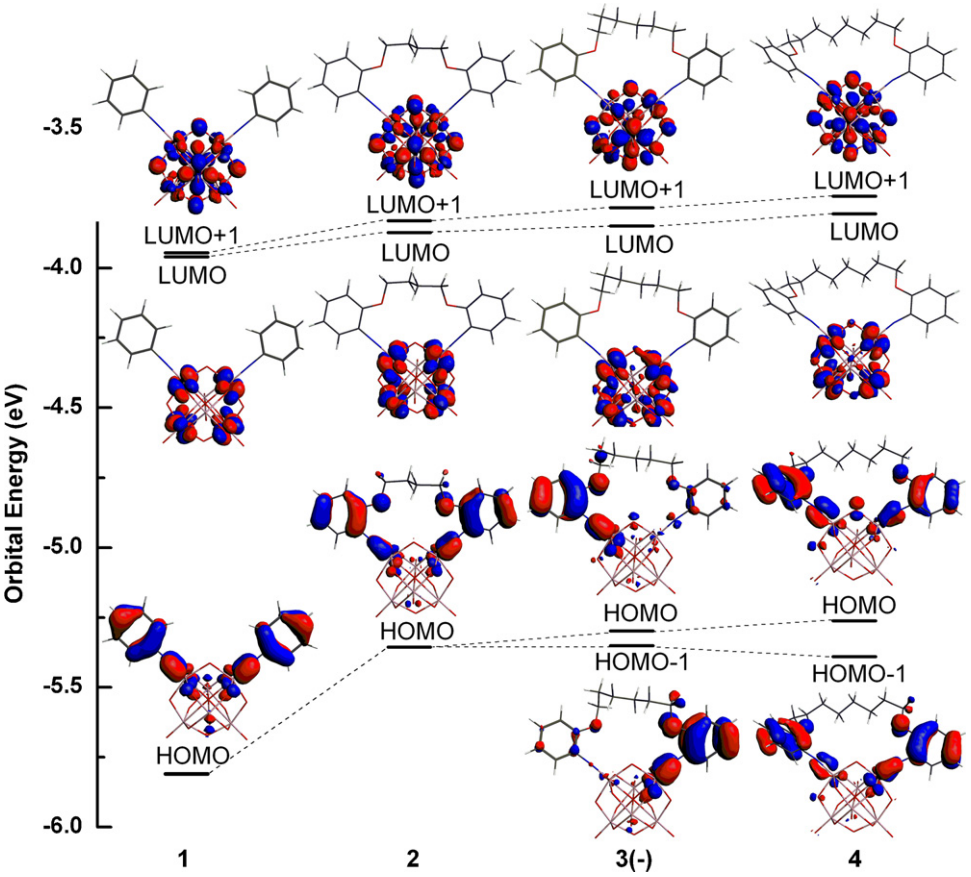

Fig. 3. The frontier molecular orbital energy diagram for systems **1**, **2**, **3**(−), and **4**.

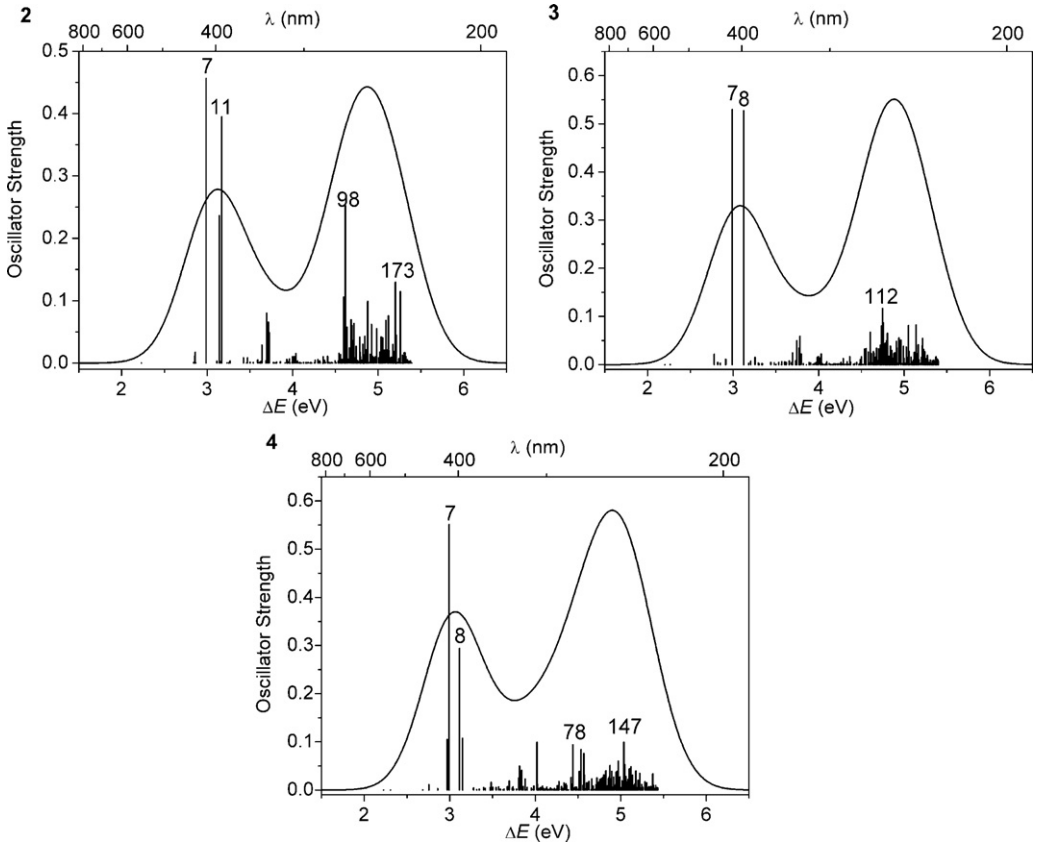

Fig. 4. The calculated UV-Vis spectra of systems **2**, **3**(−), and **4**. The half bandwidth at half peak height $\gamma = 0.4$ eV.

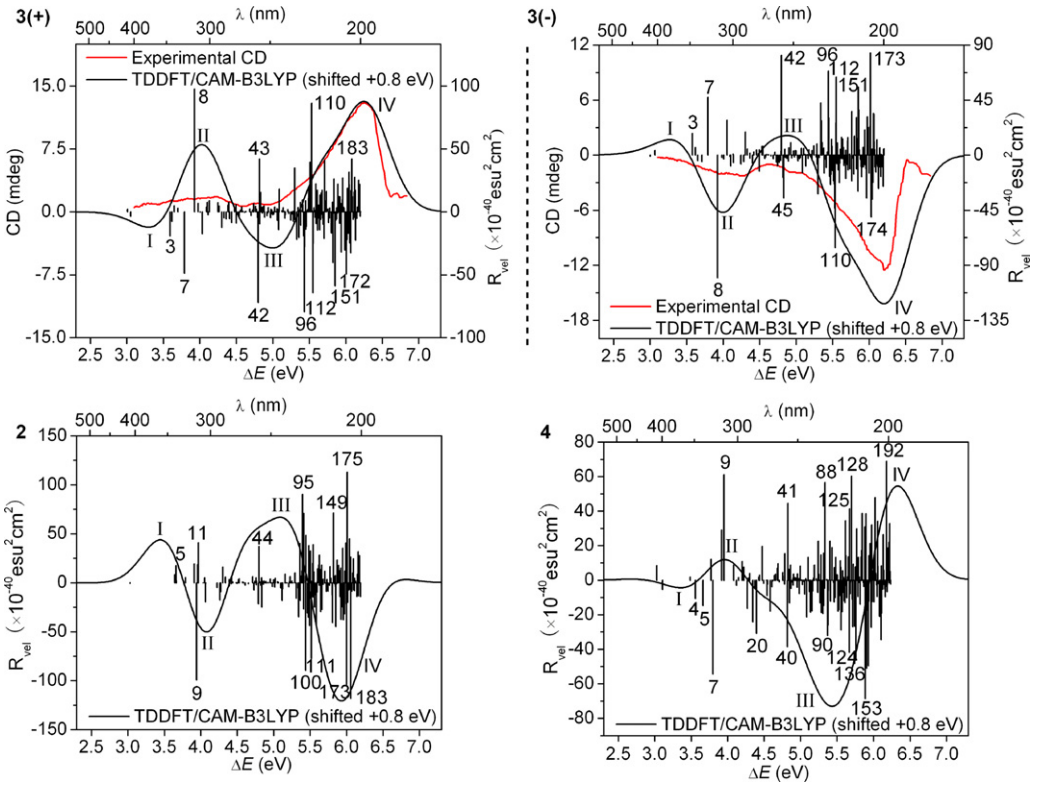

Fig. 5. The ECD spectra of systems **2**, **3**(±), and **4**. The calculated ECD spectra are uniformly shifted +0.8 eV. The experimental data were obtained from reference [43]. The half bandwidth at half peak height $\gamma = 0.4$ eV.

excited states 95, 98, 173, and 183 were derived from the CT transitions from the bridging oxygen atoms to the molybdenum atoms of the POM cage (CT^2). The simulated shapes of the UV-Vis spectra of systems **3** and **4** were similar to that of system **2**. There were two intense absorptions (states 7 and 8) in the low-lying UV-Vis spectrum of system **3**. The high-lying UV-Vis band of system **3** featured a large number of compact states with weak oscillator strengths, such as state 112. The EDDMs showed that states 7 and 8 of system **3** were ascribed to CT^1 transitions, and state 112 resulted from the combination of CT^1 and CT^2 transitions. For system **4**, four excited states, 6, 7, 8, and 9, were the major contributors to the low-lying UV-Vis band, and the high-lying band resulted from compact states, such as 78 and 147. The low-lying UV-Vis absorption of system **4** was ascribed to CT^1 transitions, and the high-lying band was a combination of CT^1 and CT^2 transitions.

The calculated excitation energies, the corresponding optical rotatory strengths, and the simulated and experimental ECD spectra for systems **2**, **3**(±), and **4** are shown in Fig. 5. A comparison of the theoretical spectra with the experimental spectra showed that the calculated ECD spectra were red-shifted by 0.8 eV. Though the shift was slightly larger than those reported in other works [16,22,64], it is acceptable for large systems such as POMs. This absorption site deviation from the experiment was predominantly credited to the employed small basis set. The correction of the calculated excitation energies relative to the experiment was alternatively realized in our previous work [65]. The rotatory strengths that were calculated with the dipole-velocity and dipole-length formulas deviated from each other by an average of 23% with the <5 rotatory strengths omitted, which is larger than usually required (< 10%). This indicated that the basis set was not well converged in our calculations. To obtain origin-independent rotatory strengths, the dipole-velocity form was employed [66].

Compared with the experimental spectra, the simulated ECD spectra of systems **3**(±) showed overall red-shifted peaks: a small broad band at $\Delta E \approx 2.5$ eV (band I), a small sharp band at $\Delta E \approx 3.2$ eV (band II), a small broad band at $\Delta E \approx 4.2$ eV (band III), and a strong sharp band at $\Delta E \approx 5.5$ eV (band VI). Herein, ECD bands I and III were negative for **3(+)** and positive for **3**(−), while bands II and IV were positive for **3(+)** and negative for **3**(−). The ECD bands I and II of **3**(±) were the optical rotatory absorptions that corresponded to the low-lying UV-Vis band at $\Delta E \approx 3.2$ eV, and bands III and IV corresponded to the UV-Vis absorptions at $\Delta E \approx 4.8$ eV. The ECD bands I and II of **3**(±) were assigned to the low-lying experimental CD spectra over $\Delta E \approx 3$–4.5 eV. ECD band I of **3**(±) was simulated from excited states 1 and 3, and band II was simulated from opposite-sign states, such as states 7 and 8. According to the EDDMs of these states, the origins of bands I and II were ascribed to CT^1 transitions (Fig. 6 and Supplementary File). This suggested that the entire chiral POM is an optically active chromophore [59]. ECD bands III and IV of **3**(±) were assigned to the experimental CD band over $\Delta E \approx 4.5$–7.0 eV. ECD band III of **3**(±) was simulated from the opposite-sign optical rotatory absorptions, which mainly corresponded to excited states 42 and 43 for **3(+)** and states 42 and 45 for **3**(−). Given that the enantiomers displayed opposite signs and equal magnitudes of rotatory strengths, the slight magnitude differences between ECD bands III and IV in enantiomers **3**(±) were ascribed to the torsion angle φ deviations, which were also observed experimentally (Table 1). The shape of ECD band IV for **3**(±) agreed well with the experimental band, which meant that both the signs and the magnitudes of the optical rotatory strengths over this range were well predicted by our calculations. Band IV of **3**(±) was simulated from the compact opposite-sign optical rotatory absorptions that corresponded to excited states, such as 96, 110, 112, and 151. The EDDMs of these states showed that the combination of CT^1 and CT^2 transitions contributed to ECD band IV of **3**(±).

ECD spectrum variations are always related to the differences in molecular configurations and the changes in molecular

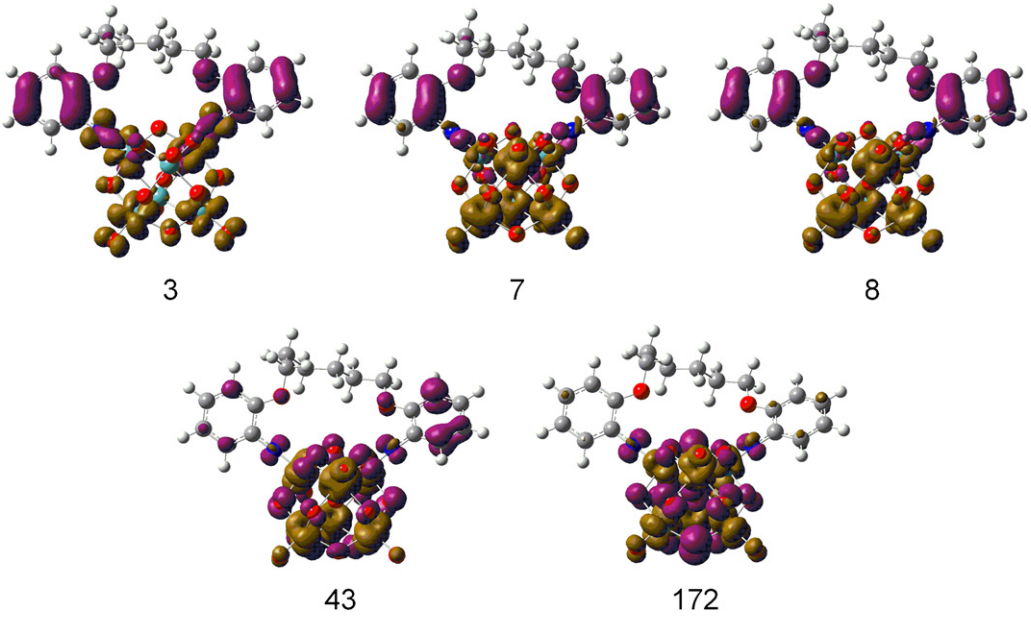

Fig. 6. The EDDMs for excited states 3, 7, 8, 43, and 172 of system **3**(+).

conformations for chiral molecules. To determine the effects of o-alkoxy chains on the ECD spectra of our systems, the ECD spectra of systems **2** and **4** were further predicted. The ECD absorption sites of system **2** were similar to those of system **3**(−), while the magnitudes of the rotatory strengths were different. These included two opposite-sign weak bands at $\Delta E \approx 2.7$ eV (band I, positive) and $\Delta E \approx 3.3$ eV (band II, negative), a weak broad band at $\Delta E \approx 4.2$ eV (band III, positive), and a strong sharp band at $\Delta E \approx 5.1$ eV (band IV, negative). For system **2**, band I was mainly simulated from the positive rotatory absorption corresponding to excited state 5, band II was simulated from opposite-sign rotatory absorptions related to excited states 9 and 11, and band III was simulated from state 44. The EDDMs showed that excited states 5, 9, 11, and 44 were ascribed to CT^1 transitions (Supplementary File). The ECD band IV of system **2** was simulated from the opposite rotatory strengths that corresponded to compact CT^1 and CT^2 excitations, such as excited states 95, 100, 111, 149, 173, 175, and 183. Compared with systems **2** and **3**(±), the rotatory strengths of system **4** were weak, which included a small broad band at $\Delta E \approx 2.6$ eV (band I, negative), a small band at $\Delta E \approx 3.2$ eV (band II, positive), a strong broad band at $\Delta E \approx 4.1$ eV (band III, negative), and a strong sharp band at $\Delta E \approx 5.5$ eV (band IV, positive). The EDDMs showed that ECD bands I and II of system **4** were ascribed to CT^1 transitions, and bands III and IV were from the combination of CT^1 and CT^2 transitions.

Therefore, the simulated ECD spectra of systems **2**, **3**(±), and **4** were slightly varied with regard to their absorption sites but largely differed in the signs and magnitudes of their rotatory strengths. They displayed two pairs of Cotton effects, which corresponded to two excited absorptions at $\Delta E \approx 3.2$ eV and $\Delta E \approx 4.8$ eV in the UV-Vis spectra [59]. The o-alkoxy chains were not involved in the electronic transitions of the studied systems. However, the ECD contributions stemming from the POM cage were of great interest. The chirality of the POM cage was deduced from the bond length alternations of Mo-O-Mo, which were induced by the intramolecular tension originating from the twisted chiral o-alkoxy chain through the two aromatic rings. The chirality transfer into the POM cage was confirmed by the rotatory absorptions that corresponded to CT^2 transitions, such as excited states 43 and 172 (Fig. 6). These transitions predominantly contributed to the high-lying ECD spectra of the studied systems.

4. Conclusions

In this paper, we investigated the geometric structures, the electronic properties, and the ECD spectra of chiral bisarylimidos bearing different lengths of o-alkoxy chain-substituted POMs. The results showed that the geometries of these macrocyclic polyanions were confirmed to be relatively rigid in solution and close to their crystal structures, which led to their intramolecular chirality. The ECD spectra of the studied chiral POMs predominantly varied in the signs and the magnitudes of their rotatory strengths while manifesting similar absorption sites. The low-lying ECD spectra of the studied chiral POMs originated from charge-transfer transitions from arylimido fragments to the POM cages, while the high-lying bands were from charge-transfer transitions from arylimido fragments to POM cages and from oxygen atoms to the molybdenum atoms in the POM cages. The o-alkoxy chain served as a scaffold for generating the chirality rather than contributing to the ECD absorption bands. Chirality transfers were observed by the charge-transfer transitions that were completely localized on the POM cages.

For the ECD calculations of chiral POMs, the long-range corrected CAM-B3LYP hybrid functional and a basis set larger than Lanl2DZ should be used in the future. Our work establishes the use of computational studies to investigate the optical activities of chiral POMs and provides theoretical interpretations.

Acknowledgments

The authors thank the computational support from the Research Center of Agriculture and Medicine Gene Engineering of the Ministry of Education of Northeast Normal University. The financial support from the NSFC (20971020, 21073030 and 21131001), the Doctoral Fund of Ministry of Education of China (20100043120007), and the Science and Technology Development Planning of Jilin Province (20100104) is gratefully acknowledged. In addition, the authors thank Dr. Yu-He Kan for the computational support.

Appendix A. Supplementary data

Supplementary data associated with this article can be found, in the online version, at doi:10.1016/j.jmgm.2011.12.011.

References

[1] L. Valade, D. de Caro, M. Basso-Bert, I. Malfant, C. Faulmann, B.G. de Bonneval, J.P. Legros, Thin films of transition metal-containing molecule-based materials: a highlight on electrochemically processed systems, Coord. Chem. Rev. 249 (2005) 1986–1996.

[2] U. Kortz, A. Müller, J. van Slageren, J. Schnack, N.S. Dalal, M. Dressel, Polyoxometalates: fascinating structures unique magnetic properties, Coord. Chem. Rev. 253 (2009) 2315–2327.

[3] S. Gatard, S. Blanchard, B. Schollhorn, P. Gouzerh, A. Proust, K. Boubekeur, Electroactive benzothiazole hydrazones and their $[Mo_6O_{19}]^{2-}$ derivatives: promising building blocks for conducting molecular materials, Chem. Eur. J. 16 (2010) 8390–8399.

[4] J.-D. Compain, P. Mialane, A. Dolbecq, J.R.M. Marrot, A. Proust, K. Nakatani, P. Yu, F. Seïcheresse, Second-order nonlinear optical properties of polyoxometalate salts of a chiral stilbazolium derivative, Inorg. Chem. 48 (2009) 6222–6228.

[5] X. Fang, T.M. Anderson, C.L. Hill, Enantiomerically pure polytungstates: chirality transfer through zirconium coordination centers to nanosized inorganic clusters, Angew. Chem. Int. Ed. 44 (2005) 3540–3544.

[6] M. Carraro, G. Modugno, A. Sartorel, G. Scorrano, M. Bonchio, Optically active polyoxotungstates bearing chiral organophosphonate substituents, Eur. J. Inorg. Chem. (2009) 5164–5174.

[7] N. Dupré, P. Rémy, K. Micoine, C. Boglio, S. Thorimbert, E. Lacôte, B. Hasenknopf, M. Malacria, Chemoselective catalysis with organosoluble lewis acidic polyoxotungstates, Chem. Eur. J. 16 (2010) 7256–7264.

[8] M. Sadakane, M.H. Dickman, M.T. Pope, Chiral polyoxotungstates. 1. Stereoselective interaction of amino acids with enantiomers of $[Ce^{III}(\alpha_1\text{-}P_2W_{17}O_{61})(H_2O)_x]^{7-}$. The structure of DL-$[Ce_2(H_2O)_8(P_2W_{17}O_{61})_2]^{14-}$, Inorg. Chem. 40 (2001) 2715–2719.

[9] K. Micoine, B. Hasenknopf, S. Thorimbert, E. Lacote, M. Malacria, Chiral recognition of hybrid metal oxide by peptides, Angew. Chem. Int. Ed. 48 (2009) 3466–3468.

[10] V. Soghomonian, Q. Chen, R.C. Haushalter, J. Zubieta, C.J. O'Connor, An inorganic double helix: hydrothermal synthesis structure, and magnetism of chiral $[(CH_3)_2NH_2]K_4[V_{10}O_{10}(H_2O)_2(OH)_4(PO_4)_7]\cdot 4H_2O$, Science 259 (1993) 1596–1599.

[11] Y. Hou, X. Fang, C.L. Hill, Breaking symmetry: spontaneous resolution of a polyoxometalate, Chem. Eur. J. 13 (2007) 9442–9447.

[12] J. Zhang, J. Hao, Y. Wei, F. Xiao, P. Yin, L. Wang, Nanoscale chiral rod-like molecular triads assembled from achiral polyoxometalates, J. Am. Chem. Soc. 132 (2010) 14–15.

[13] C. Jahier, M. Cantuel, N.D. McClenaghan, T. Buffeteau, D. Cavagnat, F. Agbossou, M. Carraro, M. Bonchio, S. Nlate, Enantiopure dendritic polyoxometalates: chirality transfer from dendritic wedges to a POM cluster for asymmetric sulfide oxidation, Chem. Eur. J. 15 (2009) 8703–8708.

[14] H.Y. An, E.B. Wang, D.R. Xiao, Y.G. Li, Z.M. Su, L. Xu, Chiral 3D architectures with helical channels constructed from polyoxometalate clusters and copper-amino acid complexes, Angew. Chem. Int. Ed. 45 (2006) 904–908.

[15] B. Hasenknopf, K. Micoine, E. Lacote, S. Thorimbert, M. Malacria, R. Thouvenot, Chirality in polyoxometalate chemistry, Eur. J. Inorg. Chem. 2008 (2008) 5001–5013.

[16] A. Sánchez-Castillo, C. Noguez, I.L. Garzón, On the origin of the optical activity displayed by chiral-ligand-protected metallic nanoclusters, J. Am. Chem. Soc. 132 (2010) 1504–1505.

[17] S.J. Wezenberg, G. Salassa, E.C. Escudero-Adain, J. Benet-Buchholz, A.W. Kleij, Effective chirogenesis in a bis(metallosalphen) complex through host–guest binding with carboxylic acids, Angew. Chem. Int. Ed. (2010), doi:10.1002/anie.201006805.

[18] S. Shima, S. Vogt, A. Göbels, E. Bill, Iron-chromophore circular dichroism of [Fe]-hydrogenase: the conformational change required for H_2 activation, Angew. Chem. Int. Ed. 49 (2010) 9917–9921.

[19] M. Lu, J. Kang, D.G. Wang, Z.H. Peng, Enantiopure 1,1′-binaphthyl-based polyoxometalate-containing molecular hybrids, Inorg. Chem. 44 (2005) 7711–7713.

[20] G. Yang, J. Li, Y. Liu, T.L. Lowary, Y. Xu, Determination of the absolute configurations of bicyclo[3.1.0]hexane derivatives via electronic circular dichroism optical rotation dispersion and vibrational circular dichroism spectroscopy and density functional theory calculations, Org. Biomol. Chem. 8 (2010) 3777–3783.

[21] G. Yang, Y. Xu, J. Hou, H. Zhang, Y. Zhao, Determination of the absolute configuration of pentacoordinate chiral phosphorus compounds in solution by using vibrational circular dichroism spectroscopy and density functional theory, Chem. Eur. J. 16 (2010) 2518–2527.

[22] J. Fan, T. Ziegler, On the origin of circular dichroism in trigonal dihedral cobalt (III) Complexes of unsaturated bidentate ligands, Inorg. Chem. 47 (2008) 4762–4773.

[23] J. Fan, J. Autschbach, T. Ziegler, Electronic structure and circular dichroism of tris(bipyridyl) metal complexes within density functional theory, Inorg. Chem. 49 (2010) 1355–1362.

[24] C.G. Liu, W. Guan, P. Song, Z.M. Su, C. Yao, E.B. Wang, Second-order nonlinear optical properties of trisubstituted Keggin and Wells-Dawson polyoxometalates: density functional theory investigation of the inorganic donor-conjugated bridge-acceptor structure, Inorg. Chem. 48 (2009) 8115–8119.

[25] L. Yan, G. Yang, W. Guan, Z. Su, R. Wang, Density functional theory study on the first hyperpolarizabilities of organoimido derivatives of hexamolybdates, J. Phys. Chem. B 109 (2005) 22332–22336.

[26] G.C. Yang, W. Guan, L.K. Yan, Z.M. Su, L. Xu, E.B. Wang, Theoretical study on the electronic spectrum and the origin of remarkably large third-order nonlinear optical properties of organoimide derivatives of hexamolybdates, J. Phys. Chem. B 110 (2006) 23092–23098.

[27] C. Diedrich, S. Grimme, Systematic investigation of modern quantum chemical methods to predict electronic circular dichroism spectra, J. Phys. Chem. A 107 (2003) 2524–2539.

[28] F.J. Coughlin, K.D. Oyler, R.A. Pascal Jr., S. Bernhard, Determination of absolute configuration of chiral hemicage metal complexes using time-dependent density functional theory, Inorg. Chem. 47 (2008) 974–979.

[29] J. Autschbach, Density functional theory applied to calculating optical and spectroscopic properties of metal complexes: NMR and optical activity, Coord. Chem. Rev. 251 (2007) 1796–1821.

[30] T. Yanai, D.P. Tew, N.C. Handy, A new hybrid exchange-correlation functional using the coulomb-attenuating method (CAM-B3LYP), Chem. Phys. Lett. 393 (2004) 51–57.

[31] O. Julinek, V. Setnicka, N. Miklasova, M. Putala, K. Ruud, M. Urbanova, Determination of molecular structure of bisphenylene homologues of BINOL-based phosphoramidites by chiroptical methods, J. Phys. Chem. A 113 (2009) 10717–10725.

[32] R. Kobayashi, R.D. Amos, The application of CAM-B3LYP to the charge-transfer band problem of the zincbacteriochlorin-bacteriochlorin complex, Chem. Phys. Lett. 420 (2006) 106–109.

[33] M.J.G. Peach, A.J. Cohen, D.J. Tozer, Influence of coulomb-attenuation on exchange-correlation functional quality, Phys. Chem. Chem. Phys. 8 (2006) 4543–4549.

[34] M.J.G. Peach, T. Helgaker, P. Salek, T.W. Keal, O.B. Lutnaes, D.J. Tozer, N.C. Handy, Assessment of a coulomb-attenuated exchange-correlation energy functional, Phys. Chem. Chem. Phys. 8 (2006) 558–562.

[35] N. Govind, M. Valiev, L. Jensen, K. Kowalski, Excitation energies of zinc porphyrin in aqueous solution using long-range corrected time-dependent density functional theory, J. Phys. Chem. A 113 (2009) 6041–6043.

[36] J. Guthmuller, L. Gonzalez, Simulation of the resonance Raman intensities of a ruthenium-palladium photocatalyst by time dependent density functional theory, Phys. Chem. Chem. Phys. 12 (2010) 14812–14821.

[37] B.X. Tian, E.S.E. Eriksson, L.A. Eriksson, Can range-separated and hybrid DFT functionals predict low-lying excitations? A Tookad case study, J. Chem. Theory Comput. 6 (2010) 2086–2094.

[38] A.H. Pakiari, Z. Jamshidi, Nature and strength of M—S bonds (M═Au Ag, and Cu) in binary alloy gold clusters, J. Phys. Chem. A 114 (2010) 9212–9221.

[39] R. Bjornsson, M. Buhl, Electric field gradients of transition metal complexes from density functional theory: assessment of functionals, geometries and basis sets, J. Chem. Soc. Dalton Trans. 39 (2010) 5319–5324.

[40] C. Thierfelder, P. Schwerdtfeger, T. Saue, Cu-63 and Au-197 nuclear quadrupole moments from four-component relativistic density-functional calculations using correct long-range exchange, Phys. Rev. A 76 (2007) 034502.

[41] M. Buhl, B. Wrackmeyer, Density-functional computation of Nb-93 NMR chemical shifts, Magn. Reson. Chem. 48 (2010) S61–S68.

[42] H.Y. Cheng, J.T. Chang, C.C. Shih, Application of the stabilization method to temporary anion states of π-ligand transition-metal carbonyls in density functional theory, J. Phys. Chem. A 114 (2010) 2920–2929.

[43] F. Xiao, J. Hao, J. Zhang, C. Lv, P. Yin, L. Wang, Y. Wei, Polyoxometalatocyclophanes: controlled assembly of polyoxometalate-based chiral metallamacrocycles from achiral building blocks, J. Am. Chem. Soc. 132 (2010) 5956–5957.

[44] ADF2008.01 (SCM, Theoretical Chemistry, Vrije Universiteit, Amsterdam, The Netherlands, http://www.scm.com).

[45] C. Fonseca Guerra, J.G. Snijders, G. te Velde, E.J. Baerends, Towards an order-N DFT method, Theor. Chem. Acc. 99 (1998) 391–403.

[46] G. te Velde, F.M. Bickelhaupt, E.J. Baerends, C. Fonseca Guerra, S.J.A. van Gisbergen, J.G. Snijders, T. Ziegler, Chemistry with ADF, J. Comput. Chem. 22 (2001) 931–967.

[47] M.J. Frisch, G.W. Trucks, H.B. Schlegel, G.E. Scuseria, M.A. Robb, J.R. Cheeseman, G. Scalmani, V. Barone, B. Mennucci, G.A. Petersson, H. Nakatsuji, M. Caricato, X. Li, H.P. Hratchian, A.F. Izmaylov, J. Bloino, G. Zheng, J.L. Sonnenberg, M. Hada, M. Ehara, K. Toyota, R. Fukuda, J. Hasegawa, M. Ishida, T. Nakajima, Y. Honda, O. Kitao, H. Nakai, T. Vreven, J.A. Montgomery Jr., J.E. Peralta, F. Ogliaro, M. Bearpark, J.J. Heyd, E. Brothers, K.N. Kudin, V.N. Staroverov, R. Kobayashi, J. ormand, K. Raghavachari, A. Rendell, J.C. Burant, S.S. Iyengar, J. Tomasi, M. Cossi, N. Rega, J.M. Millam, M. Klene, J.E. Knox, J.B. Cross, V. Bakken, C. Adamo, J. Jaramillo, R. Gomperts, R.E. Stratmann, O. Yazyev, A.J. Austin, R. Cammi, C. Pomelli, J.W. Ochterski, R.L. Martin, K. Morokuma, V.G. Zakrzewski, G.A. Voth, P. Salvador, J.J. Dannenberg, S. Dapprich, A.D. Daniels, O. Farkas, J.B. Foresman, J.V. Ortiz, J. Cioslowski, D.J. Fox, Gaussian 09, Revision A.01, Gaussian, Inc., Wallingford, CT, 2009.

[48] S.H. Vosko, L. Wilk, M. Nusair, Accurate spin-dependent electron liquid correlation energies for local spin density calculations: a critical analysis, Can. J. Phys. 58 (1980) 1200–1211.

[49] A.D. Becke, Density-functional exchange-energy approximation with correct asymptotic behavior, Phys. Rev. A 38 (1988) 3098–3100.

[50] J.P. Perdew, Density-functional approximation for the correlation energy of the inhomogeneous electron gas, Phys. Rev. B 33 (1986) 8822–8824.

[51] E. van Lenthe, E.J. Baerends, J.G. Snijders, Relativistic regular two-component Hamiltonians, J. Chem. Phys. 99 (1993) 4597–4610.

[52] C.C. Pye, T. Ziegler, An implementation of the conductor-like screening model of solvation within the Amsterdam density functional package, Theor. Chem. Acc. 101 (1999) 396–408.
[53] J.P. Wang, L.K. Yan, W. Guan, S.Z. Wen, Z.M. Su, The structure-property relationship of chiral 1,1′-binaphthyl-based polyoxometalates: TDDFT studies on the static first hyperpolarizabilities and the ECD spectra, J. Mol. Graphics Modell. (2011), doi:10.1016/j.jmgm.2011.09.005.
[54] P.J. Hay, W.R. Wadt, Ab initio effective core potentials for molecular calculations. Potentials for the transition metal atoms Sc to Hg, J. Chem. Phys. 82 (1985) 270–283.
[55] W.R. Wadt, P.J. Hay, Ab initio effective core potentials for molecular calculations. Potentials for main group elements Na to Bi, J. Chem. Phys. 82 (1985) 284–298.
[56] J. Autschbach, F.E. Jorge, T. Ziegler, Density functional calculations on electronic circular dichroism spectra of chiral transition metal complexes, Inorg. Chem. 42 (2003) 2867–2877.
[57] J. Kongsted, T.B. Pedersen, A. Osted, A.E. Hansen, K.V. Mikkelsen, O. Christiansen, Solvent effects on rotatory strength tensors. 1. Theory and application of the combined coupled cluster/dielectric continuum model, J. Phys. Chem. A 108 (2004) 3632–3641.
[58] J. Tomasi, B. Mennucci, R. Cammi, Quantum mechanical continuum solvation models, Chem. Rev. 105 (2005) 2999–3094.
[59] R.D. Peacock, B. Stewart, Circular dichroism of transition metal complexes, Coord. Chem. Rev. 46 (1982) 129–157.
[60] M. Pecul, K. Ruud, A. Rizzo, T. Helgaker, Conformational effects on the optical rotation of alanine and proline, J. Phys. Chem. A 108 (2004) 4269–4276.
[61] D. Andrae, U. Häußermann, M. Dolg, H. Stoll, H. Preuß, Energy-adjusted ab initio pseudopotentials for the second and third row transition elements, Theor. Chim. Acta 77 (1990) 123–141.
[62] F. Weigend, R. Ahlrichs, Balanced basis sets of split valence triple zeta valence and quadruple zeta valence quality for H to Rn: design and assessment of accuracy, Phys. Chem. Chem. Phys. 7 (2005) 3297–3305.
[63] N.M. O'Boyle, A.L. Tenderholt, K.M. Langner, cclib: a library for package-independent computational chemistry algorithms, J. Comp. Chem. 29 (2008) 839–845.
[64] S.B. Graule, M. Rudolph, N. Vanthuyne, J. Autschbach, C. Roussel, J. Crassous, R.G. Reĭau, Metal-bis(helicene) assemblies incorporating (-conjugated phosphole-azahelicene ligands: impacting chiroptical properties by metal variation, J. Am. Chem. Soc. 131 (2009) 3183–3185.
[65] T. Gao, L.L. Shi, H.B. Li, S.S. Zhao, H. Li, S.L. Sun, Z.M. Su, Y.H. Lu, Improving the accuracy of low level quantum chemical calculation for absorption energies: the genetic algorithm and neural network approach, Phys. Chem. Chem. Phys. 11 (2009) 5124–5129.
[66] T.D. Crawford, M.C. Tam, The current state of ab initio calculations of optical rotation and electronic circular dichroism spectra, J. Phys. Chem. A 111 (2007) 12057–12068.